J. Water Environ. Nanotechnol., 6(4): 367-378 Autumn 2021

ORIGINAL RESEARCH PAPER

Synthesis, characterization and photocatalytic application of $ZnWO_4/ZrO_2$ nanocomposite towards degradation of methyl orange dye

K. Buvaneswari[1*], R. Arunadevi[2*], S. Sashikala[2], K. Kavipriya[3]

[1] P.G. Department of Chemistry, Sri S.Ramasamy Naidu Memorial College, Sattur- 626203. Tamilnadu, India.
[2] P.G and Research Department of Chemistry, D.K.M.College for Women (Autonomous), Vellore-632001, Tamilnadu, India.
[3] Department of Chemistry, Thiravium College of Arts and Science for Women, Periyakulam, Theni(Dt), Tamilnadu, India.

Received: 2021-04-17 Accepted: 2021-06-28 Published: 2021-08-01

ABSTRACT

Visible light active $ZnWO_4/ZrO_2$ nanocomposite was prepared via hydrothermal method. The nanocomposite was characterized by UV-visible diffuse reflectance spectroscopy (UV-vis-DRS), Fourier transforms infrared spectroscopy (FT-IR), X-ray diffraction (XRD), Scanning Electron microscopy (SEM), energy-dispersive X-ray spectroscopy (EDX), and transmission electron microscopy (TEM) techniques. The XRD results showed that the average particle size of ZrO2, $ZnWO_4$, and $ZnWO_4/ZrO_2$ was found to be 29.20 nm, 23.78 nm, and 20.14 nm respectively and the phase structure for ZrO_2 and $ZnWO_4$ in the composite was Rhombohedral and Monoclinic respectively. The UV–vis absorption spectra of the $ZnWO_4/ZrO_2$ nanocomposite noticeably shifted to the visible light region compared to that of the ZrO_2. The prepared photocatalyst was composed of a plate and spongy sphere with little agglomeration was seen from the SEM result. The photocatalytic activities of the prepared nanocomposite were evaluated for the degradation of methyl orange (MO) under visible light irradiations. The effect of operational parameters such as initial dye concentration, pH, catalyst concentration, and irradiation time has been investigated in detail. The photocatalytic degradation efficiency of $ZnWO_4/ZrO_2$, $ZnWO_4$ and ZrO_2 for 95%, 72%, and 60 % respectively. The high photocatalytic activity can be attributed to stronger absorption in the visible light region, a greater specific surface area, smaller crystal sizes, more surface OH groups, and to the effect of $ZnWO_4$ doping, which resulted in lower bandgap energy

Keywords: *$ZnWO_4/ZrO_2$, photocatalysis, visible light, methyl orange*

How to cite this article
Buvaneswari K., Arunadevi R., Sashikala S., Kavipriya K. Synthesis, characterization and photocatalytic application of $ZnWO_4/ZrO_2$ nanocomposite towards degradation of methyl orange dye. J. Water Environ. Nanotechnol., 2021; 6(4): 367-378.
DOI: 10.22090/jwent.2021.04.007

INTRODUCTION

Visible light responding photocatalysts have been widely investigated for the degradation of various pollutants [1–3] water splitting [4,5] and photoelectrochemical (PEC) cells [6,7]. A number of these photocatalysts do perform adequately under visible light. This is due to an unfavorable balance between the enhanced visible light absorption and a negative impact on charge recombination [8]. Recently, many studies have highlighted the way of coupling a wide band-gap semiconductor (with the proper band positions) to form a junction structure, which has been found to enhance the charge separation, leading to

* Corresponding Author Email: *arunarajan3@gmail.com*
bhuvanasrnmc@gmail.com

improvement of photocatalytic activity [9–13].

ZrO_2 is an n-type semiconductor, with a wide bandgap and large negative value of the conduction band [14–16]. The photocatalytic activity of ZrO_2 is usually investigated at around 250 nm, but studies were carried out for some samples in the range between 290–390 nm [17]. It was also reported that ZrO_2 showed photocatalytic activity at 320 nm, due to the absorption band emerging from an impurity level [18]. ZrO_2 was used in the oxidation of 2-propanoltoacetone [19], in the photocatalytic degradation of 4-chlorophenol, 4-nitrophenol, and methylene blue [20–22]. But, due to its limitation factor of the high percentage of electron-hole recombination and practical difficulties, various methods have been explored for ZrO_2 material [23].

Tungstate nanomaterials with novel architectures and physical and chemical properties are very useful for many potential applications such as flashing materials, LED, magnetic and fluorescent materials, light-emitting materials, photocatalytic materials, scintillator, laser host, and nanoordered substrate materials, so they are considered as an important class of functional materials. As an important photocatalyst, $ZnWO_4$ has been applied for photocatalytic hydrogen production from water and mineralization of organic pollutants under UV light irradiation.

Azo dyes, especially methyl orange, are mainly used in the textile, paper, synthetic leather, and food industry due to their high chemical stability. Methyl orange (or Sodium 4-[(4-dimethylamino) phenyldiazenyl] benzenesulfonate) is a common azo dye with features of both a dye and an acid-base indicator in aqueous solutions. Since methyl orange does not degrade easily in a conventional manner, the treatment of methyl orange in the effluent is a major challenge for the dyeing industry. In treating the printing and dyeing wastewater, methyl orange of a certain concentration is selected as a typical degradation compound.

Moreover, to reduce the electron-hole recombination and completely contribute to the redox process, that can couple with other visible light responding photocatalysts for further charge transfer. $ZnWO_4$, a novel visible responding photocatalyst with a 3.40 eV band gap, has been extensively used to degrade organic compounds due to its highly efficient oxidation ability and changeable morphologies [24-26]. Herein, we demonstrate a convenient hydrothermal method at room temperature for the synthesis of novel $ZnWO_4/ZrO_2$ nanoparticles. The synthesized nanoparticles are carefully characterized using UV-vis DRS, FTIR, XRD, SEM, EDX, BET, and TEM techniques. Also, the photocatalytic activity of the $ZnWO_4/ZrO_2$ nanoparticles in the degradation of methyl orange (MO) is investigated.

EXPERIMENTAL

Preparation of photocatalyst

Analytical grade Zinc acetate, Sodium Tungstate, Zirconium Oxy Chloride, Sodium Hydroxide, Ethanol were purchased from Merck (India) and used without purification. Double distilled water was used in the photocatalytic experiments.

Preparation of ZrO_2

In a typical experimental procedure, 5 g of $ZrOCl_2.8H_2O$ was dissolved in 90 ml distilled water. This solution was stirred for 2 h. The pH of the solution was maintained at pH 12 by adding 10% NaOH solution. The resulting suspension was refluxed and heated to 60 °C for 2 h. The solution was gradually cooled to room temperature. The resultant white precipitate was washed several times and dried at 60 °C for 1 h in a hot air oven. The above precipitate was calcinated in a muffle furnace at 600 °C for 2 h.

Preparation of $ZnWO_4$

$ZnWO_4$ was prepared by dissolving 5 g of Zinc acetate in 50 ml distilled water. 4.3 g of Sodium Tungstate dissolved in 50 ml distilled water was added to the above solution with constant stirring. Then the mixture was stirred for 2 h. The obtained precipitate was washed with distilled water several times and dried in a hot air oven at 120 °C for 1 h. The obtained $ZnWO_4$ was calcinated in a muffle furnace at 500 °C for 1 h.

Preparation of $ZnWO_4/ZrO_2$ nanocomposite

2 g of ZrO_2 and 0.5084 g of $ZnWO_4$ were dissolved in 100 ml of ethanol. The whole mixture was sonicated for 30 minutes, refluxed for 2 h, and stirred for 2 h. Then the precipitate was washed with ethanol solution and dried at 60 °C for 1 h. It was calcinated in a muffle furnace at 500°C for 2 h to obtain $ZnWO_4/ZrO_2$ nanocomposite [27].

Photocatalytic activity experiments

Photocatalytic experiments were carried out in an immersion-type photoreactor. 300 ml of MO

with an initial concentration of 10 µm was taken in a cylindrical glass vessel which was surrounded by a circulating water jacket to cool the lamp. The air was bubbled continuously into the aliquot by an air pump in order to provide a constant source of dissolved oxygen. Before irradiation, the reaction mixture was stirred in dark for 15 minutes to achieve the adsorption-desorption equilibrium between the catalyst and dye molecules [28, 29]. 300 W Xe lamp with an ultraviolet cut-off filter was used as the visible light radiation, 5ml of aliquot was collected at regular time intervals. Then the sample was centrifuged to remove the photocatalyst and the filtrate was analyzed by UV-vis spectrophotometer at maximum absorption of 464 nm. The photodegradation of MO was calculated by the formula given below.

$$\text{Photo deg radation}(\%)\text{ of MO} = \frac{C_0 - C}{C_0} \text{x} 100 \qquad (1)$$

Where, C_O is the concentration of MO before irradiation time, and C is the concentration of MO after a certain irradiation time.

Characterization of Photocatalyst

UV visible diffuse reflectance spectra were acquired using a Shimadzu UV-2450 spectrophotometer. $BaSO_4$ was used as the reflectance standard. The surface structure was characterized by a Fourier-transform infrared (FT-IR) spectrophotometer (JASCO-FT-IR-460 plus). X-ray diffraction (XRD) patterns of the prepared photocatalytic samples were obtained using an X-ray diffractometer (XRD; XPERT PRO X-RAY) with monochromatic Cu Kα radiation. XRD scanning was performed under ambient conditions over a 2θ region of 20°–60° at a rate of 2 °/min (40 kV, 20 mA). The surface morphology was examined using scanning electron microscopy (SEM) (JSM 6701F—6701) in both secondary and backscattered electron modes and the elemental analysis was also detected. Transmission electron microscopy (TEM) mapping images were obtained using the TEM-TECNAI G2 model. pH was monitored using a EUTECH instrument pH meter.

RESULTS AND DISCUSSION

Characterization

UV–vis DRS

The optical properties of the nanocomposite influence their photocatalytic activity. The UV-vis-DRS of ZrO_2, $ZnWO_4$, and $ZnWO_4/ZrO_2$ were shown in Fig.1 (a). It was seen from the figure that the absorption peaks for $ZnWO_4/ZrO_2$ are highly redshifted when compared to ZrO_2 and $ZnWO_4$. The optical band gap E_g of the nanoparticles was determined by extrapolation of the linear portion of α^2 versus hν plots using the following equation [30].

$$\alpha = \frac{c(h\gamma - E_g^{bulk})^2}{h\gamma} \qquad (2)$$

Where α is the absorption coefficient, hν is the photon energy, E_g is the optical band gap energy and c is the constant depending on the electron-hole mobility. Tauc plots of ZrO_2, $ZnWO_4$, and $ZnWO_4/ZrO_2$ were shown in Fig. 1(b), 1(c), and 1(d). The band gaps of ZrO_2, $ZnWO_4$, and $ZnWO_4/ZrO_2$ were found to be 3.6 eV, 3.2 eV, and 2.5 eV respectively. The bandgap of $ZnWO_4/ZrO_2$ is sharper and highly suitable for receiving visible light.

FT-IR

Fig. 2 (a), (b), and (c) shows the FT-IR spectra of ZrO_2, $ZnWO_4$, and $ZnWO_4/ZrO_2$ respectively. The absorption peaks at 761 and 890 cm^{-1} are originated from the bending and stretching vibration of Zn-O-W. The two peaks at 3473 and 1635 cm^{-1} implying that the basic hydroxyl group in nanocomposite [31] and are also attributed to stretching vibrations of the OH groups in W-OH. The Zr-O band was observed at 1064 cm^{-1}. The band at 670 cm^{-1} was due to a Zr-O bending vibration. Peaks that occurred less than 610 cm^{-1} belong to Zr-O band vibrations. The surface OH group density increases with tungsten incorporation. The larger surface hydroxyl group density will lead to the enhancement of the photocatalytic activity because they can interact with photogenerated holes, which gives better charge transfer and inhibits the recombination of electron-hole pairs [32, 33].

XRD

The phase composition of ZrO_2, $ZnWO_4$, and $ZnWO_4/ZrO_2$ were shown in Fig.3. The observed peaks of the nanocomposite were in good consistency with the characteristic peaks of ZrO_2 (based on a JCPDS card no 730958) with Rhombohedral phase and Rhombo-centered lattice) and $ZnWO_4$ (based on a JCPDS card no 880251) with Monoclinic phase and Primitive

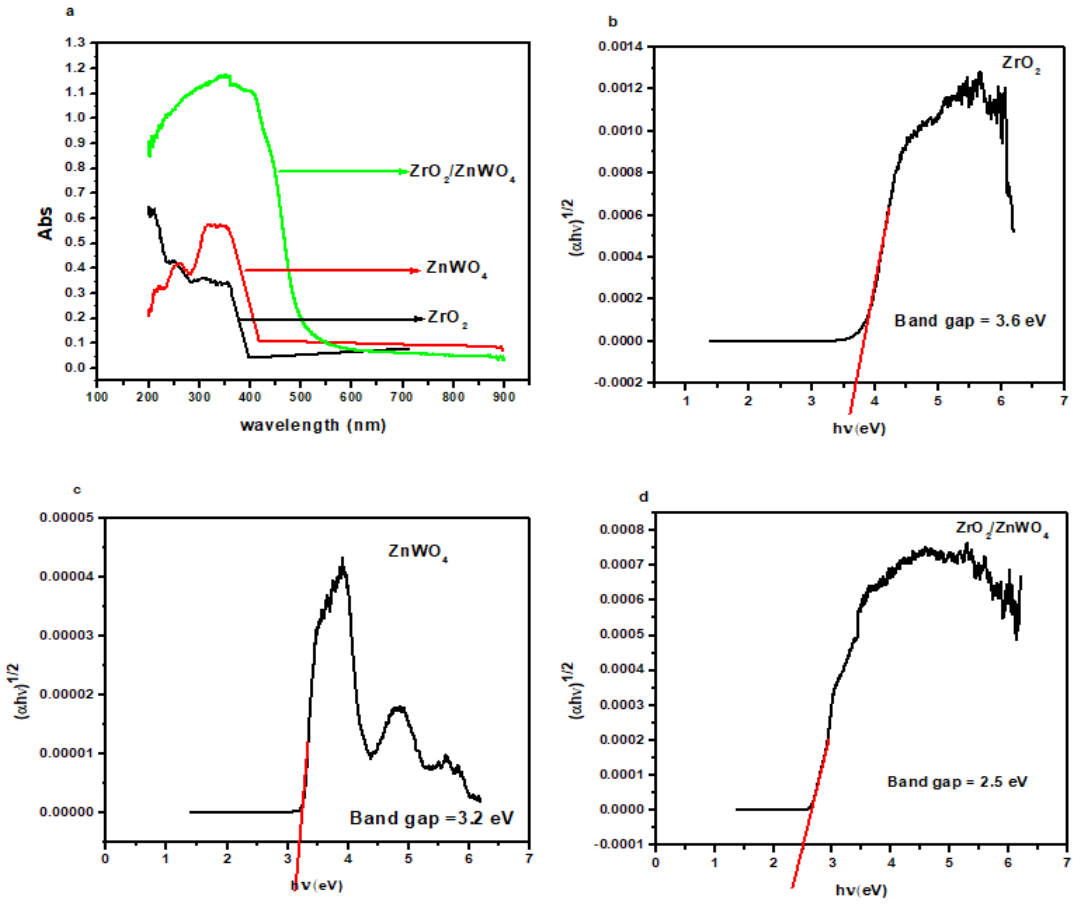

Fig. 1. (a). UV – vis -DRS spectra of ZrO_2, $ZnWO_4$ and $ZnWO_4/ZrO_2$, (b) Tauc plot of ZrO_2, (c) Tauc plot $ZnWO_4$, (d) Tauc plot $ZnWO_4/ZrO_2$

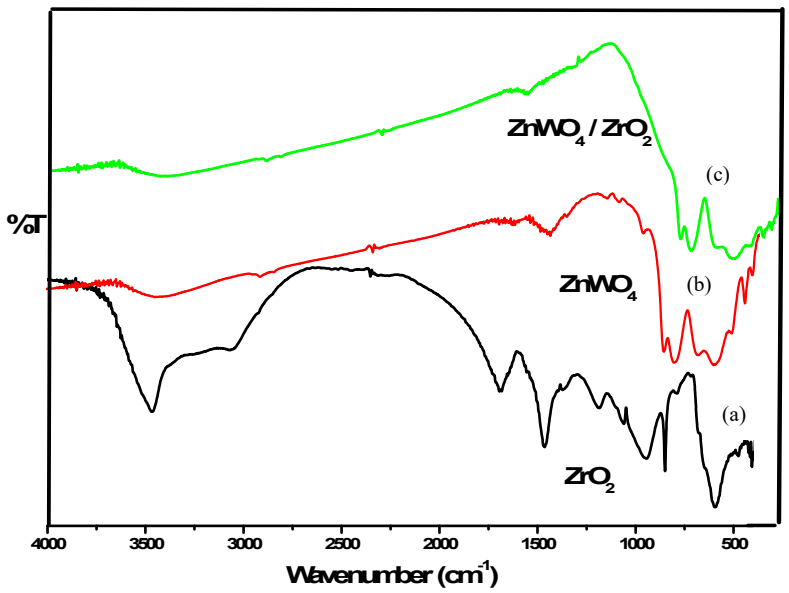

Fig. 2. FT-IR spectra of ZrO_2, $ZnWO_4$ and $ZnWO_4/ZrO_2$

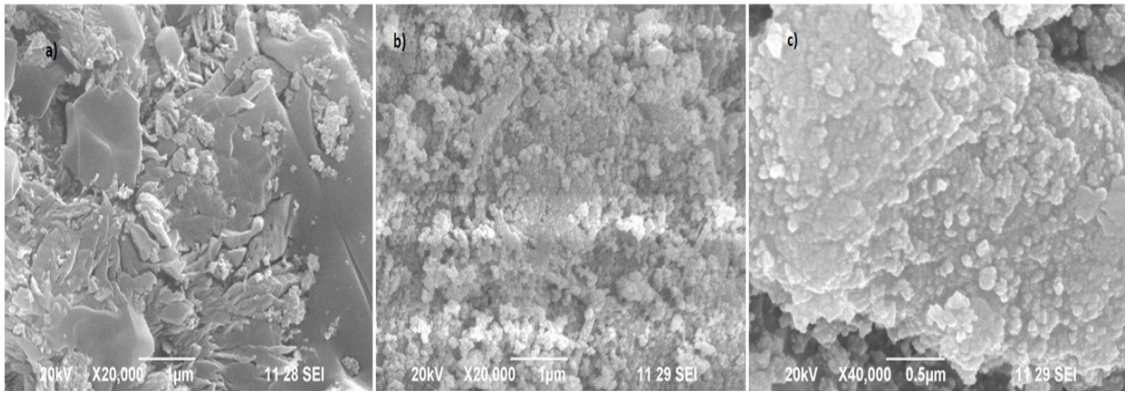

Fig. 4.(a) SEM image of ZrO_2, (b) SEM image of $ZnWO_4$, (c) SEM image of $ZnWO_4/ZrO_2$

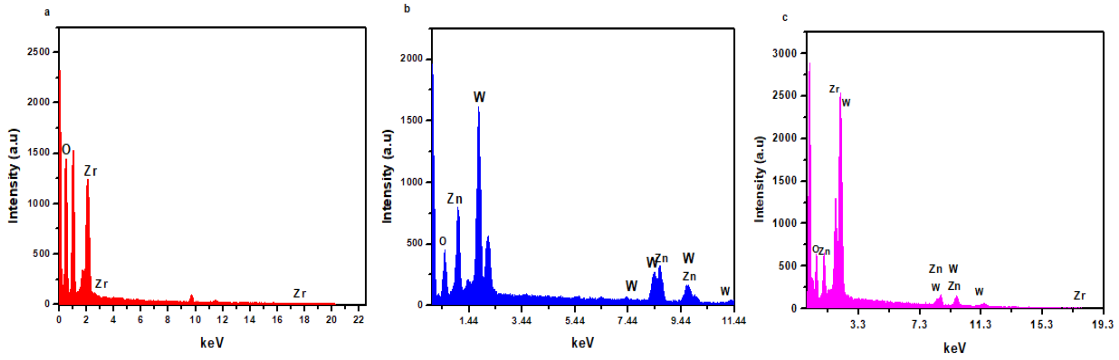

Fig.5. (a) EDX of ZrO_2 ,) (b) EDX of $ZnWO_4$, (c) EDX of $ZnWO_4/ZrO_2$

lattice). The average crystallize size was calculated using the Debye-Scherrer equation [34]

$$D = \frac{K\lambda}{\beta Cos\theta} \quad (3)$$

Where β is the full width at half height maximum of the most intense 2θ peak, K is the shape factor (0.89). θ, λ are the incident angle and wavelength of X – rays respectively. The average particle size obtained for ZrO_2, $ZnWO_4$, and $ZnWO_4/ZrO_2$ nanoparticles were found to be 29.20 nm, 23.78 nm, and 20.14 nm respectively.

SEM, EDX, and TEM

The surface morphology of ZrO_2, $ZnWO_4$, and $ZnWO_4/ZrO_2$ was observed by SEM and shown in Fig. 4 (a), 4 (b), 4 (c) respectively. Plate-like morphology was observed for ZrO_2 and spongy sphere for $ZnWO_4$ [35]. On doping with $ZnWO_4$, ZrO_2 shows agglomeration. The compositions of ZrO_2, $ZnWO_4$, and $ZnWO_4/ZrO_2$ nanocomposite were determined by EDX shown in Fig.5.(a),(b) and (c) respectively. The EDX result shows that the sample containing Zr, Zn, W, and O were observed at their energy levels without any impurities The EDX elemental analysis of ZrO2, ZnWO4, and ZnWO4/ZrO2 is given in Table. 1. TEM image of nanocomposite was shown in Fig.6. It was observed to be a plate with sponge spheres and the average crystallization was found to be 28-39 nm which is in good agreement with the XRD results.

Photocatalytic activity

Photocatalytic degradation of MO

Fig.7. shows the photocatalytic activity of ZrO_2, $ZnWO_4$, and $ZnWO_4/ZrO_2$ for the degradation of MO (Reaction conditions: MO 1.5 μM and catalyst concentration 0.125 g/L). The results revealed that the degradation of MO has only achieved 30% in the presence of $ZnWO_4$ and 23% of MO is degraded by ZrO_2. However, the highest photocatalytic activity is shown by $ZnWO_4/ZrO_2$ (95%). The photodegradation of MO was also

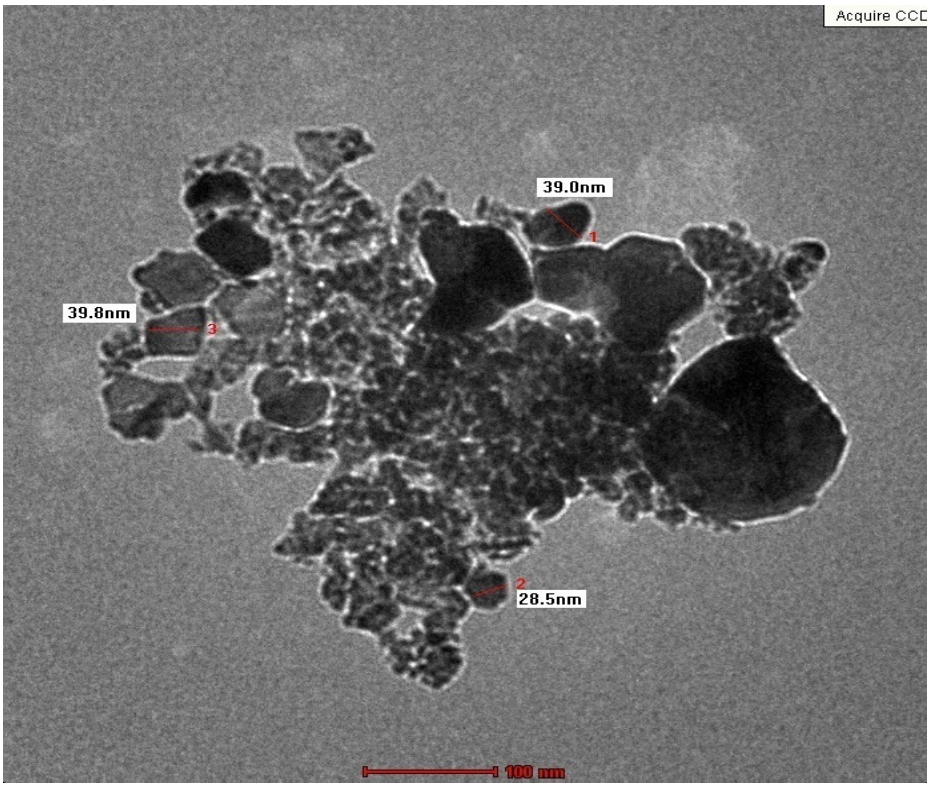

Fig. 6. TEM image of ZnWO4/ZrO_2

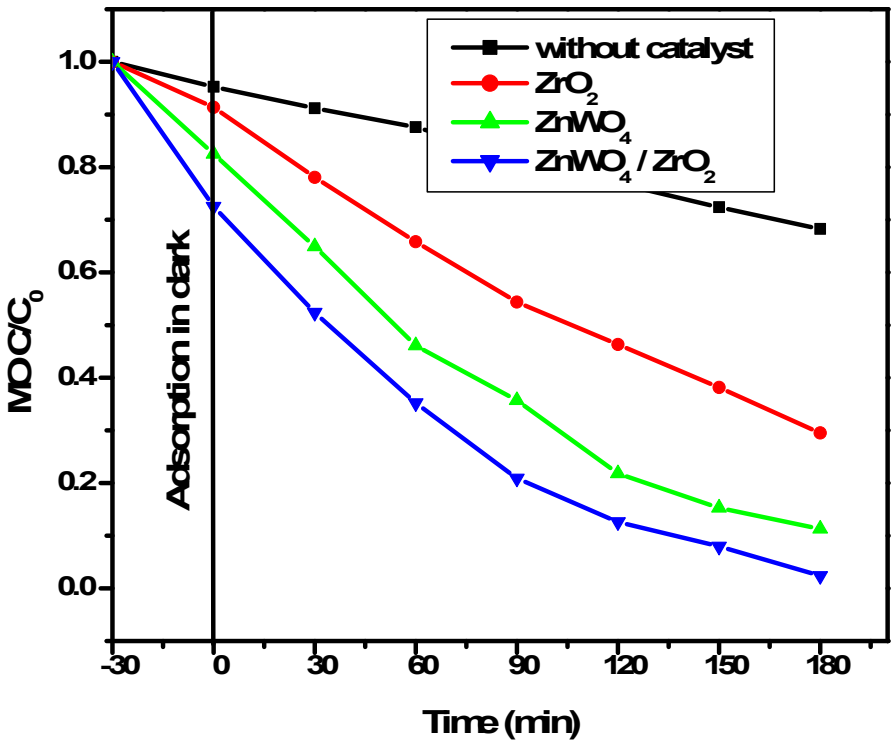

Fig. 7. Photodegradation of MO in the presence of ZrO_2, $ZnWO_4$, and $ZnWO_4/ZrO_2$

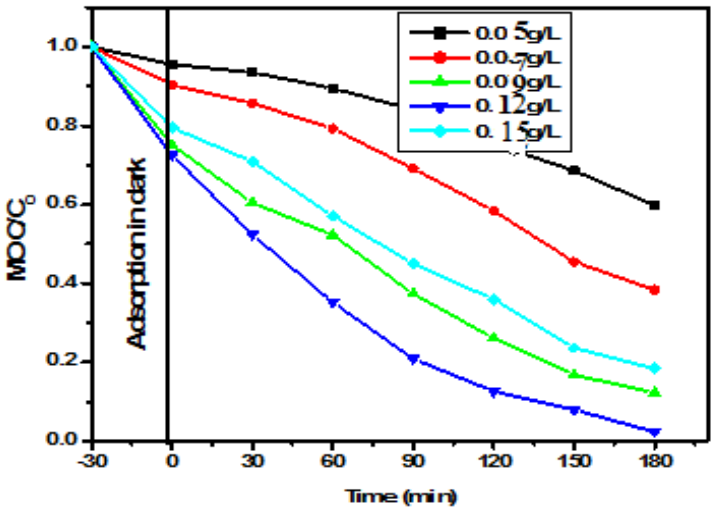

Fig. 8. Effect of catalyst dosage on photodegradation of MO

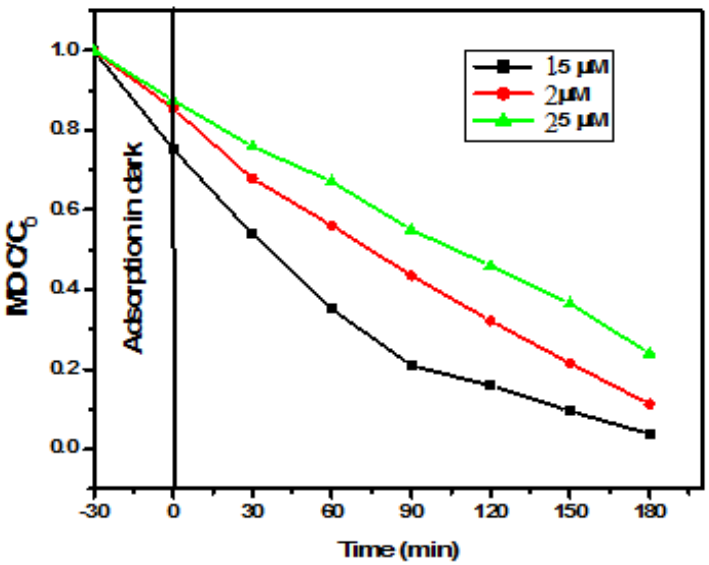

Fig. 9. Effect of concentration of MO and its photodegradation

carried out without light (only catalyst) for up to 180 min. The adsorption percentage of the MO at 180 min of contact time is negligible (16%) without nanocomposites.

The highest photocatalytic activity of $ZnWO_4/ZrO_2$ can be explained as follows: when the photocatalyst is irradiated with visible light, electrons and holes are formed in the conduction band and valence band of $ZnWO_4/ZrO_2$ (narrow bandgap semiconductor). Therefore photogenerated electrons of $ZnWO_4$ will be easily transferred to the conduction band of ZrO_2 (wide bandgap semiconductor). Therefore, efficient electron-hole separation is achieved on the photocatalyst surface. The electron reacts with surface adsorbed O_2 to produce $O_2^{\cdot-}$ and holes react with H_2O to create $^{\cdot}OH$. This results in more charge carriers forming reactive species, which promote the degradation of MO [36].

Effect of Catalyst dosage

In order to optimize the photocatalyst dosage on the degradation of MO, experiments were carried out with varying $ZnWO_4/ZrO_2$ dosage from 0.050 g/L to 0.150 g/L, at a constant MO concentration of 1.5 µM and the results are shown in Fig. 8. The

Table. 1. EDX elemental analysis of ZrO_2, $ZnWO_4$ and $ZnWO_4/ZrO_2$

S.no	Samples	Atomic %	keV
1	ZrO_2	Zr= 21.13	Zr= 3.8 keV
		O = 78.87	O = 0.5 keV
2	$ZnWO_4$	Zn = 15.13	Zn = 7.93keV
		W = 14.00	W = 3.821keV
		O = 70.87	O = 0.5 keV
3	$ZnWO_4/ZrO_2$	Zr= 18.75	Zr = 3.8 keV
		Zn= 18.75	Zn= 7.93 keV
		W = 2.38	W =2.2, 9.8 keV
		O = 78.87	O = 0.5 keV

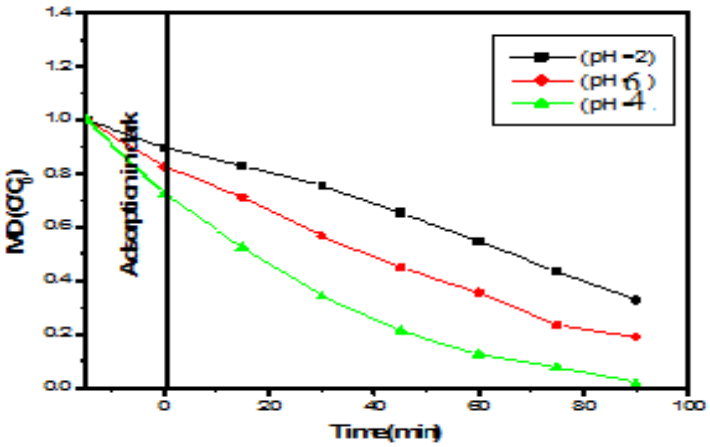

Fig. 10. Effect of pH on photodegradation of MO

photodegradation of MO is negligible (15.75%) without the addition of any photocatalyst during 180 min of irradiation. The photodegradation of MO increases with the increase of $ZnWO_4/ZrO_2$ dosage from 0.050 g/L to 0.125 g/L and then decreases. This is due to the increase of the total active surface area and the availability of the more active sites on the catalyst surface for photoreaction. However, the high catalyst dosage increases the turbidity of the suspension leading to a shielding effect on the penetration of light [37]. Therefore, the absorption of light by the photocatalyst is limited, and fewer catalyst sites can be activated. The surface area was also reduced due to the agglomeration of the nanoparticles at high photocatalyst dosage.

Effect of the initial concentration of MO

The influence of initial MO concentration on its photodegradation was examined in the presence of $ZnWO_4/ZrO_2$ (0.125 g/L) and the results are displayed in Fig.9. The photodegradation of MO decreases with an increase in MO concentration from 1.5 µM to 2.5 µM. At high MO concentrations, more MO molecules are adsorbed on the surface of $ZnWO_4/ZrO_2$ and fewer photons are available to reach the catalyst surface and therefore the less number of OH is formed, thus causing inhibition in degradation percentage. Also, an increase in MO concentration can lead to a decrease in the path length of the photon entering the aqueous solution of MO and reduce the catalytic efficiency [38].

Effect of pH

The degradation of MO was studied at different pH ranges from 2-6 with an initial MO concentration of 1.5 µM, catalyst concentration ($ZnWO_4/ZrO_2$) of 0.125 g/L, and irradiation time of 180 min. The degradation of MO as a function of pH is shown in Fig.10. The photodegradation of MO increases with an increase in pH from 2 to 4 and a further increase in pH leads to a decrease in photodegradation. The photocatalytic activity of $ZnWO_4/ZrO_2$ was found to be 95% at pH 4 [39, 40].

The kinetics of photodegradation of MO

The kinetics of photodegradation of MO was studied by conducting the experiments under optimum operation conditions (MO concentration

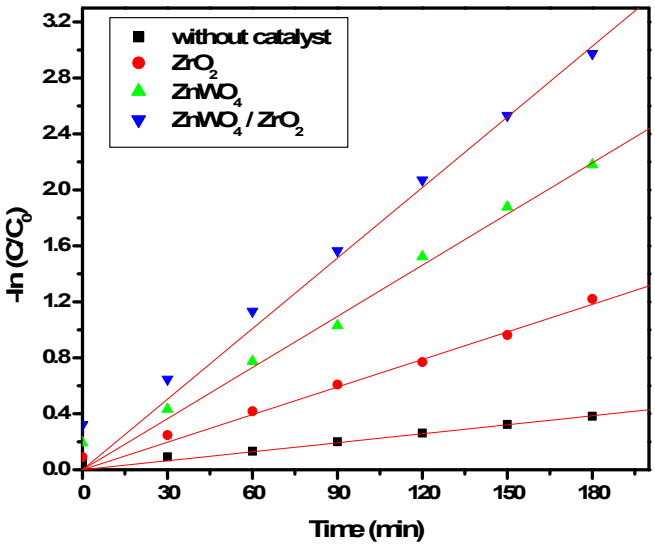

Fig.11. Kinetics regime on the photodegradation of MO in the presence of ZrO_2, $ZnWO_4$, and $ZnWO_4/ZrO_2$

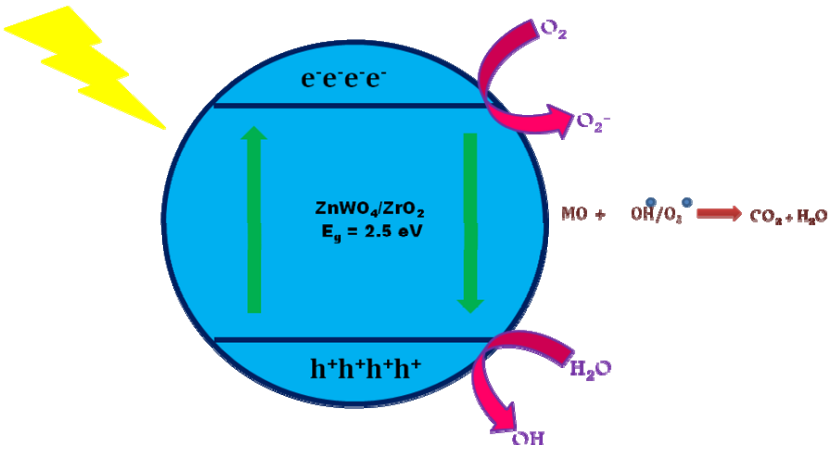

Fig.12. Mechanism of $ZnWO_4/ZrO_2$ on MO

1.5 µM, $ZnWO_4/ZrO_2$ concentration 0.125 g/L, and irradiation time 90 min). In all experiments, the degradation followed first-order kinetics plots of $-\ln[C/C_0]$ versus time showed a linear relationship, where C is the concentration of MO remaining in the solution at irradiation time of t, and C_0 is the initial concentration at t = 15 min). First-order rate constants were evaluated from the slopes of the $-\ln [C/C_0]$ versus time plots in Fig.11. [41]. The observed rate constant for the photodegradation of MO in the presence of $ZnWO_4/ZrO_2$ is $1.45x10^{-2}$ s^{-1}, which is significantly higher than that observed for ZrO_2 ($5.8x10^{-3}$ s^{-1}), $ZnWO_4$ ($1.08x10^{-2}$ s^{-1}) and without catalyst ($1.8x10^{-3}$ s^{-1}). Moreover, Fig. 12 shows the mechanism of $ZnWO_4/ZrO_2$ on MO.

Recycle ability

From Fig. 13 the study of reusability of the catalyst composite. To evaluate changes in the efficiency and kinetic constants of reused photocatalyst, 0.125 g/L of the catalyst was tested for three cycles. The dye decolorization was mildly decreasing from 92 % (1st cycle) to 90 % in the second cycle and 85 % in the third cycle. Generally, the catalyst remained sufficiently efficient after repeated use. The loss of activity of the photocatalyst might be due to the adsorption of insensitive species on the photocatalyst surface and the supporting matrix. Moreover, the comparison of methyl orange degradation efficiency for different catalysts is shown in Table 2.

Table. 2 The comparison of methyl orange degradation efficiency for different catalysts

Catalyst	Dye	% of degradation	Reference
Chitosan Embedded Nano-CdS	Methyl orange	99 %	[42]
Co:La:TiO_2 Nanocomposite	Methyl orange	98.9 %	[43]
Ferrocene appended supported ionic liquid phase (SILP) photocatalyst	Methyl orange	99%	[44]
Ag/TiO_2/biochar	Methyl orange	97.48 %	[45]
TiO_2 –Zeolite	Methyl orange	88.47 %	[46]
$ZnWO_4/ZrO_2$	Methyl orange	95%	Present study

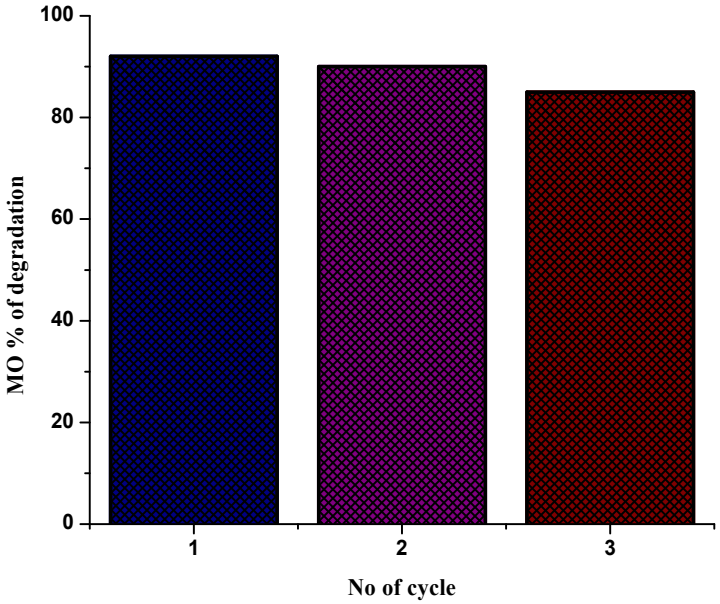

Fig. 13. Recycle ability

CONCLUSION

In this present work, $ZnWO_4/ZrO_2$ has been successfully synthesized and effectively utilized for visible-light-driven photocatalyst for the degradation of methyl orange. The prepared nanoparticles have been characterized using UV – vis DRS, FTIR, XRD, SEM, TEM, and EDX techniques. It was observed to be a plate with sponge spheres for $ZnWO_4/ZrO_2$ nanocomposite and the average crystallization was found to be 28-39 nm which is in good agreement with the XRD results. The photocatalyst was successfully applied for the degradation of MO under visible light and the reaction parameters were optimized. $ZnWO_4/ZrO_2$ (95%) shows higher photocatalytic activity than ZrO_2 (60 %) and $ZnWO_4$ (72%).

CONFLICTS OF INTEREST

There are no conflicts to declare.

REFERENCES

1. Abe R, Takami H, Murakami N, Ohtani B. Pristine Simple Oxides as Visible Light Driven Photocatalysts: Highly Efficient Decomposition of Organic Compounds over Platinum-Loaded Tungsten Oxide. Journal of the American Chemical Society. 2008;130(25):7780-1.
2. Malathy P, Vignesh K, Rajarajan M, Suganthi A. Enhanced photocatalytic performance of transition metal doped Bi2O3 nanoparticles under visible light irradiation. Ceramics International. 2014;40(1):101-7.
3. Vignesh K, Priyanka R, Rajarajan M, Suganthi A. Photoreduction of Cr(VI) in water using Bi2O3–ZrO2 nanocomposite under visible light irradiation. Materials Science and Engineering: B. 2013;178(2):149-57.
4. Maeda K, Takata T, Hara M, Saito N, Inoue Y, Kobayashi H, et al. GaN:ZnO Solid Solution as a Photocatalyst for Visible-Light-Driven Overall Water Splitting. Journal of the American Chemical Society. 2005;127(23):8286-7.
5. Maeda K, Domen K. New Non-Oxide Photocatalysts Designed for Overall Water Splitting under Visible Light. The Journal of Physical Chemistry C. 2007;111(22):7851-61.
6. Le Formal F, Grätzel M, Sivula K. Controlling Photoactivity in Ultrathin Hematite Films for Solar Water-Splitting. Ad-

vanced Functional Materials. 2010;20(7):1099-107.
7. Baker DR, Kamat PV. Photosensitization of TiO2Nanostructures with CdS Quantum Dots: Particulate versus Tubular Support Architectures. Advanced Functional Materials. 2009;19(5):805-11.
8.X. Zhang, K. Udawa, Z. Liu, S. Nishimoto, C. Xu, Y. Lu, H. Sakai, M. Ave, T. Marakoi, A. Kujishima, Synthesis and characterization of BN/Bi_2WO_6 composite photocatalysts with enhanced visible-light photocatalytic activity, J.*Photochem. Photobio A*., 202 (2009) 39–47.
9. Kim H-i, Kim J, Kim W, Choi W. Enhanced Photocatalytic and Photoelectrochemical Activity in the Ternary Hybrid of CdS/TiO2/WO3 through the Cascadal Electron Transfer. The Journal of Physical Chemistry C. 2011;115(19):9797-805.
10.G.Colon, S.Murcia Lopez, M.C.Hidalgo, Synthesis of nanostructured ZnO/Bi_2WO_6 heterojunction for photocatalysis application *J. A. Navo, Chem. Commun*., 46 (2010) 4809–4811.
11. Min Y, Zhang K, Chen Y, Zhang Y. Synthesis of novel visible light responding vanadate/TiO2 heterostructure photocatalysts for application of organic pollutants. Chemical Engineering Journal. 2011;175:76-83.
12. Yu J, Zhang J, Jaroniec M. Preparation and enhanced visible-light photocatalytic H2-production activity of CdS quantum dots-sensitized Zn1−xCdxS solid solution. Green Chemistry. 2010;12(9):1611.
13. Hu Y, Li D, Zheng Y, Chen W, He Y, Shao Y, et al. BiVO4/TiO2 nanocrystalline heterostructure: A wide spectrum responsive photocatalyst towards the highly efficient decomposition of gaseous benzene. Applied Catalysis B: Environmental. 2011;104(1-2):30-6.
14. Neppolian B, Wang Q, Yamashita H, Choi H. Synthesis and characterization of ZrO2–TiO2 binary oxide semiconductor nanoparticles: Application and interparticle electron transfer process. Applied Catalysis A: General. 2007;333(2):264-71.
15. Wu C, Zhao X, Ren Y, Yue Y, Hua W, Cao Y, et al. Gas-phase photo-oxidations of organic compounds over different forms of zirconia. Journal of Molecular Catalysis A: Chemical. 2005;229(1-2):233-9.
16. Botta SG, Navío JA, Hidalgo MaC, Restrepo GM, Litter MI. Photocatalytic properties of ZrO2 and Fe/ZrO2 semiconductors prepared by a sol–gel technique. Journal of Photochemistry and Photobiology A: Chemistry. 1999;129(1-2):89-99.
17. Mendive CB, Bahnemann DW, Blesa MA. Microscopic characterization of the photocatalytic oxidation of oxalic acid adsorbed onto TiO2 by FTIR-ATR. Catalysis Today. 2005;101(3-4):237-44.
18. Lukáč J, Klementová M, Bezdička P, Bakardjieva S, Šubrt J, Szatmáry L, et al. Influence of Zr as TiO2 doping ion on photocatalytic degradation of 4-chlorophenol. Applied Catalysis B: Environmental. 2007;74(1-2):83-91.
19.J. A. Navio, G. Colon, J. M. Herrmann, Photoconductive and photocatalytic properties of $ZrTiO_4$, J.Photochem. Photobiol. A: Chem., 108 (1997) 179–185.
20. Al-Sayyed G, D'Oliveira J-C, Pichat P. Semiconductor-sensitized photodegradation of 4-chlorophenol in water. Journal of Photochemistry and Photobiology A: Chemistry. 1991;58(1):99-114.
21. Navío JA, Colón G, Macías M, Sánchez-Soto PJ, Augugliaro V, Palmisano L. ZrO2-SiO2 mixed oxides: surface aspects, photophysical properties and photoreactivity for 4-nitrophenol oxidation in aqueous phase. Journal of Molecular Catalysis A: Chemical. 1996;109(3):239-48.
22. Liqiang J, Yichun Q, Baiqi W, Shudan L, Baojiang J, Libin Y, et al. Review of photoluminescence performance of nano-sized semiconductor materials and its relationships with photocatalytic activity. Solar Energy Materials and Solar Cells. 2006;90(12):1773-87.
23. Vinu R, Polisetti S, Madras G. Dye sensitized visible light degradation of phenolic compounds. Chemical Engineering Journal. 2010;165(3):784-97.
24.L. Qiang, H. Fu, Preparation of c-axis oriented $LiNb_{1-x}Ta_xO_3$ films on Si(1 1 1)substrates by a modified sol–gel process, *Chem. J. Chin. Univ*., 18 (2002) 255–257.
25.Y. Liu, H. Wang, G. Chen, Analysis of Raman spectra of $ZnWO_4$ single crystals, J. *Appl. Phys*., 64 (1988) 4651–4653.
26.F. Wen, X. Zhao, Hydrothermal synthesis and photoluminescent properties of $ZnWO_4$ and Eu^{3+} doped $ZnWO_4$, J. *Chem. Mater. Lett*., 55 (2002) 152–157.
27. Vignesh K, Suganthi A, Rajarajan M, Sakthivadivel R. Visible light assisted photodecolorization of eosin-Y in aqueous solution using hesperidin modified TiO2 nanoparticles. Applied Surface Science. 2012;258(10):4592-600.
28. Vignesh K, Suganthi A, Rajarajan M, Sara SA. Photocatalytic activity of AgI sensitized ZnO nanoparticles under visible light irradiation. Powder Technology. 2012;224:331-7.
29. Nair MG, Nirmala M, Rekha K, Anukaliani A. Structural, optical, photo catalytic and antibacterial activity of ZnO and Co doped ZnO nanoparticles. Materials Letters. 2011;65(12):1797-800.
30.G.Voicu,O.Oprea,B.S.Vasile,E.Andronescu,Photoluminescenceand photocatalytic activity of Mn-doped ZnO nanoparticles, J.. *Nanomater. Bios*., 8 (2013) 667-675.
31. Komarneni S, Roy R, Li QH. Microwave-hydrothermal synthesis of ceramic powders. Materials Research Bulletin. 1992;27(12):1393-405.
32.L.Shi, K.C.Tin, N.B.Wong, Thermal stability of zirconia membranes. *J. mater. Sci.,* 34 (1999) 3367 – 3374.
33. Cabañas A, Darr JA, Lester E, Poliakoff M. Continuous hydrothermal synthesis of inorganic materials in a near-critical water flow reactor; the one-step synthesis of nano-particulate Ce1 − xZrxO2 (x = 0–1) solid solutions. Journal of Materials Chemistry. 2001;11(2):561-8.
34. Subash B, Krishnakumar B, Pandiyan V, Swaminathan M, Shanthi M. An efficient nanostructured Ag2S–ZnO for degradation of Acid Black 1 dye under day light illumination. Separation and Purification Technology. 2012;96:204-13.
35.Z. L. Liu, H. B. Wang, Q. H. Lu, G. H. Du, L. Peng, Y. Q. Du, S. M. Zhang, K. L. Yao, Synthesis and characterization of ultrafine well-dispersed magnetic 414 nanoparticles, *J. Magn. Mater.,* 283 (2004) 258–262.
36.K.Vignesh, M.Rajarajan, A.Suganthi, Photodegradation of methylene blue using Ni and Th co-doped ZnO nanoparticles under visible light, J. *Ind. Eng. Chem.*, 20 (2014) 3826-3833.
37. Yeung KL, Yau ST, Maira AJ, Coronado JM, Soria J, Yue PL. The influence of surface properties on the photocatalytic activity of nanostructured TiO2. Journal of Catalysis. 2003;219(1):107-16.
38. Lu X, Song C, Jia S, Tong Z, Tang X, Teng Y. Low-temperature selective catalytic reduction of NOX with NH3 over cerium and manganese oxides supported on TiO2–graphene. Chemical Engineering Journal. 2015;260:776-84.

39. Karthiga R, Kavitha B, Rajarajan M, Suganthi A. Photocatalytic and antimicrobial activity of NiWO4 nanoparticles stabilized by the plant extract. Materials Science in Semiconductor Processing. 2015;40:123-9.
40. Sudrajat H, Babel S, Sakai H, Takizawa S. Rapid enhanced photocatalytic degradation of dyes using novel N-doped ZrO 2. Journal of Environmental Management. 2016;165:224-34.
41. Zhang F, Zhao J, Shen T, Hidaka H, Pelizzetti E, Serpone N. TiO2-assisted photodegradation of dye pollutants II. Adsorption and degradation kinetics of eosin in TiO2 dispersions under visible light irradiation. Applied Catalysis B: Environmental. 1998;15(1-2):147-56.
42. Szeto W, Kan CW, Yuen CWM, Chan S-W, Lam KH. Effective Photodegradation of Methyl Orange Using Fluidized Bed Reactor Loaded with Cross-Linked Chitosan Embedded Nano-CdS Photocatalyst. International Journal of Chemical Engineering. 2014;2014:1-16.
43. K A, P G. Photodegradation of Methyl Orange in Aqueous Solution by the Visible Light Active Co:La:TiO2 Nanocomposite. Chemical Sciences Journal. 2017;08(03).
44. Naikwade AG, Jagadale MB, Kale DP, Gophane AD, Garadkar KM, Rashinkar GS. Photocatalytic Degradation of Methyl Orange by Magnetically Retrievable Supported Ionic Liquid Phase Photocatalyst. ACS Omega. 2020;5(1):131-44.
45. Shan R, Lu L, Gu J, Zhang Y, Yuan H, Chen Y, et al. Photocatalytic degradation of methyl orange by Ag/TiO2/biochar composite catalysts in aqueous solutions. Materials Science in Semiconductor Processing. 2020;114:105088.
46. Aziztyana AP, Wardhani S, Prananto YP, Purwonugroho D, Darjito. Optimisation of Methyl Orange Photodegradation Using TiO2-Zeolite Photocatalyst and H2O2 in Acid Condition. IOP Conference Series: Materials Science and Engineering. 2019;546(4):042047.